BMC Pharmacology and Toxicology

RESEARCH Open Access

Identification of key therapeutic targets in nicotine-induced intracranial aneurysm through integrated bioinformatics and machine learning approaches

Qiang Ma[1], Longnian Zhou[1] and Zhongde Li[1*]

Abstract

Background Intracranial aneurysm (IA) is a critical cerebrovascular condition, and nicotine exposure is a known risk factor. This study delves into the toxicological mechanisms of nicotine in IA, aiming to identify key biomarkers and therapeutic targets.

Methods Gene Set Variation Analysis (GSVA), Weighted Gene Co-Expression Network Analysis (WGCNA), and enrichment analyses were conducted on differentially expressed genes (DEGs) from the GSE122897 dataset. Additionally, nicotine-related targets were identified using CTD, SwissTargetPrediction, and Super-PRED databases. Integrative machine learning approaches, such as Random Forest (RF) and Support Vector Machine (SVM), were employed to pinpoint key toxicity targets. Molecular docking and immune cell infiltration analyses were also performed.

Results DEGs in IA showed significant alterations in metabolic, secretory, signaling, and homeostatic pathways. Several immune and metabolic response pathways were notably disrupted. WGCNA identified 1127 DEGs with 37 overlapping toxic targets between IA and nicotine. ssGSEA revealed substantial upregulation in immune response and inflammation-related processes. Integrative analyses highlighted TGFB1, MCL1, and CDKN1A as core toxicity targets, confirmed via molecular docking studies. Immune cell infiltration analysis indicated significant correlations between these core targets and various immune cell populations.

Conclusion This study uncovers significant disruptions in metabolic and immune pathways in IA under nicotine influence, identifying TGFB1, MCL1, and CDKN1A as critical biomarkers. These findings offer a deeper understanding of IA's molecular mechanisms and potential therapeutic targets for nicotine-related toxicity.

Keywords Cerebral aneurysm, Bioinformatics, Nicotine toxicity, Molecular docking, Machine learning, Cigarette smoking

*Correspondence:
Zhongde Li
lizhongde01231@aliyun.com
[1]Department of Neurosurgery II, Hexi University Affiliated Zhangye People's Hospital, No. 67 Xihuan Road, Ganzhou District, Zhangye, Gansu Province 734000, China

Introduction

Intracranial aneurysm (IA) is a significant vascular condition characterized by the abnormal dilation of blood vessels in the brain, which poses considerable risks including rupture and subarachnoid hemorrhage [1, 2]. Such events can lead to devastating neurological deficits or even death, making IA a critical focus of medical research. The societal costs associated with IA are substantial, including healthcare expenditures and loss of productivity due to debilitating outcomes [3]. Current treatment modalities, such as surgical clipping and endovascular coiling, present challenges including complications and recurrence rates, underscoring the necessity for improved targeted therapies and prevention [4, 5]. Despite advances in treatment, the recurrence of IA and its associated complications remain a significant challenge.

IA is associated with a range of genetic, environmental, and lifestyle factors, with smoking being recognized as a significant risk factor for its development and rupture [6–8]. However, while the link between smoking and IA is well-established, the precise molecular mechanisms by which nicotine contributes to IA formation and rupture remain poorly understood. Identifying molecular biomarkers and therapeutic targets for nicotine-induced IA could help mitigate the risks associated with this condition and guide the development of targeted therapeutic interventions.

Numerous studies have implicated smoking and nicotine exposure as important contributors to IA formation and rupture. Nicotine is the main active ingredient in tobacco products. By acting on various cellular pathways, nicotine can induce vascular inflammation, oxidative stress, and endothelial dysfunction, all of which contribute to the formation and development of aneurysms [9–11]. For example, nicotine exposure has been shown to facilitate the rupture of aneurysms by exerting effects on the α7 subtype of nicotinic acetylcholine receptors located in vascular smooth muscle cells [12]. Clinical studies have also highlighted a correlation between smoking and an increased incidence of IA and its rupture [7, 13]. While these studies provide important insights into the effects of nicotine on IA, the molecular pathways that mediate these effects remain unclear, particularly concerning gene expression and cellular signaling.

The current gap in research lies in the lack of a comprehensive understanding of the molecular alterations induced by nicotine exposure in IA. Traditional research approaches often fail to capture the complexity of nicotine-induced IA, as they do not integrate genomic, transcriptomic, and toxicological data on a systems level. This gap presents a major challenge in identifying robust biomarkers and therapeutic targets that could guide clinical intervention.

Modern bioinformatics has facilitated disease diagnosis by enabling systematic analysis of complex molecular datasets by integrating multi-omics profiling and advanced computational approaches [14–16]. This addresses these challenges by employing advanced bioinformatics and machine learning techniques to systematically analyze the molecular changes in IA induced by nicotine exposure. By integrating multiple advanced bioinformatics tools, such as Gene Set Variation Analysis (GSVA), Weighted Gene Co-Expression Network Analysis (WGCNA), and enrichment analyses, to investigate gene expression changes in IA. Public databases such as Comparative Toxicogenomics Database (CTD), SwissTargetPrediction, and Super-PRED were used to identify nicotine-related targets. Integrative machine learning approaches, specifically Random Forest (RF) and Support Vector Machine (SVM), were applied to pinpoint critical toxicity targets. Additionally, molecular docking analysis and molecular dynamics simulation were conducted to examine the interaction between nicotine and key toxicity targets, while immune cell infiltration analysis was used to explore immune-related alterations in IA. Figure 1 presents the flowchart of this study.

This study has the potential to provide valuable insights for the development of targeted therapeutic strategies by uncovering the molecular mechanisms and key therapeutic targets involved in nicotine-induced IA. Identifying biomarkers such as TGFB1, MCL1, and CDKN1A may facilitate early detection and risk stratification in nicotine-exposed individuals. Moreover, understanding the immune and metabolic disruptions associated with IA could lead to novel therapeutic approaches aimed at mitigating the impact of nicotine on cerebrovascular health.

Methods

Data collection and preprocessing

We analyzed the GSE122897 dataset, which encompasses gene expression profiles obtained from 16 normal samples and 44 samples from patients with IA, sourced from the Gene Expression Omnibus (GEO) database (Table S1). The probes within this dataset were aligned with gene symbols utilizing their corresponding probe annotation files. In instances where multiple probes were associated with an identical gene symbol, the average value of these probes was calculated to denote the final expression level of that specific gene. The identification of differentially expressed genes (DEGs) between the IA cohort and the normal group was performed utilizing the limma package (version 3.22.7; usage date: 17 December 2024) [17]. The selection of DEGs was based on an adjusted p-value < 0.05.

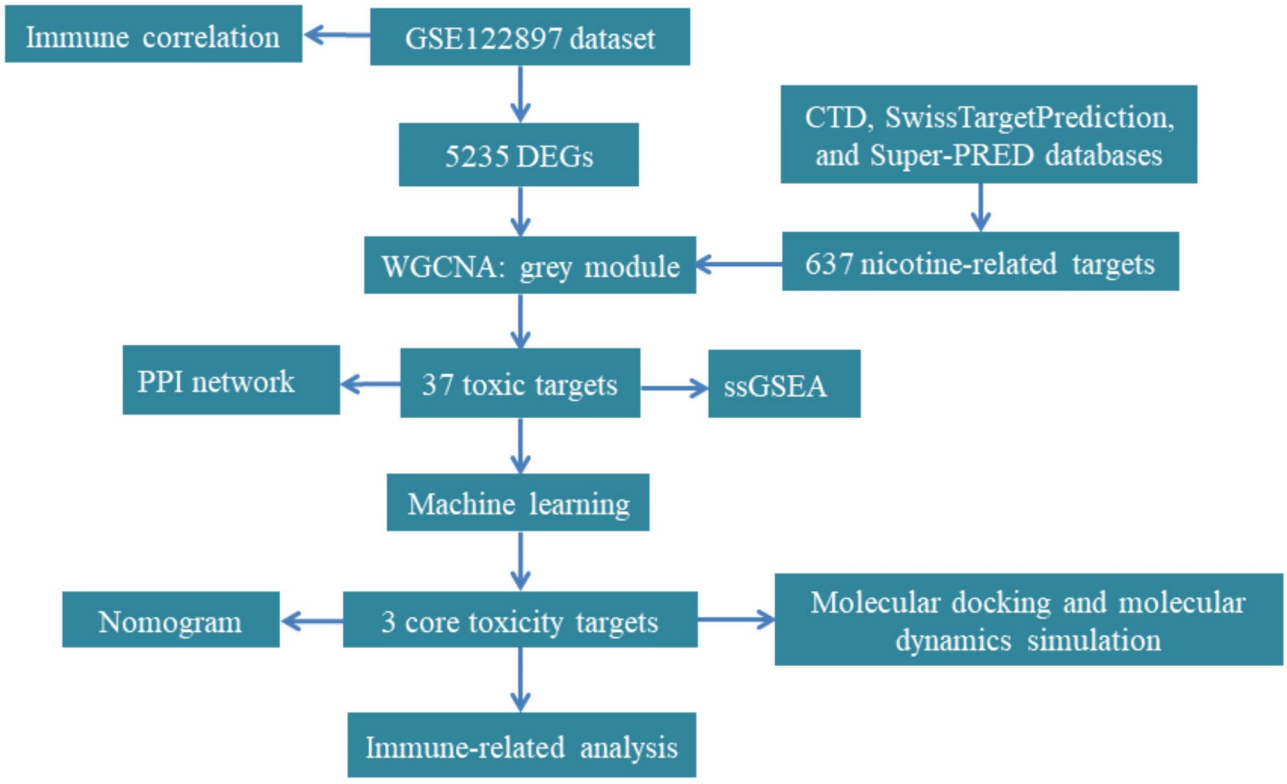

Fig. 1 Flowchart of this study

GSVA

GSVA was conducted on the DEGs using the GSVA package (version 1.50.0; usage date: 17 December 2024) in R [18]. This analysis was performed to evaluate the enrichment of biological pathways in the IA group compared to the normal group. Gene sets were selected from the Molecular Signatures Database (MSigDB), including Gene Ontology (GO) terms and Kyoto Encyclopedia of Genes and Genomes (KEGG) pathways. Pathways with a false discovery rate (FDR) of <0.05 were considered statistically significant.

WGCNA

WGCNA was performed to explore the correlation between gene expression modules and IA. The R package WGCNA (version 4.0.2; usage date: 18 December 2024) was used to construct a co-expression network based on the DEGs [19]. Modules were identified by hierarchical clustering and dynamic tree cutting. Module-trait relationships were calculated to identify the modules most strongly associated with IA. Correlations between gene significance for IA and module membership were evaluated to identify key genes within the most relevant modules.

Identification of common toxic targets between IA and nicotine exposure

To identify potential toxic targets related to nicotine exposure, we used the following databases: CTD (https://ctdbase.org/), SwissTargetPrediction (http://www.swisstargetprediction.ch/), and Super-PRED (https://prediction.charite.de/index.php) (visit date: 17 December 2024) [20, 21]. We retrieved nicotine-related targets and intersected them with the DEGs identified from the grey module in the WGCNA analysis. The overlapping targets were identified, which were further analyzed using heatmap analysis to assess their differential expression between the IA and normal groups.

Protein-protein interaction (PPI) network construction

The identified common toxic targets were analyzed for PPI using the STRING database (https://cn.string-db.org/) (visit date: 18 December 2024). A confidence score of >0.4 was set to filter reliable interactions. The PPI network was visualized using Cytoscape (version 3.8.2; usage date: 18 December 2024) and key hub proteins with the highest degree of interaction were highlighted [22].

Single-Sample Gene Set Enrichment Analysis (ssGSEA)

To investigate the molecular effects of nicotine exposure on IA, ssGSEA was applied to the 37 overlapping toxic targets using the GSVA package (version 1.50.0; usage

date: 17 December 2024) in R. This approach allowed us to assess the enrichment of biological processes and pathways at the single-sample level. The enrichment scores for various biological processes and KEGG pathways were compared between the IA and normal groups, with statistical significance determined using a Wilcoxon test ($p < 0.05$).

Machine learning analysis

To identify key toxicity targets related to nicotine exposure, machine learning algorithms, including RF and SVM, were employed. RF was performed using the randomForest R package (version 4.7.1.1; usage date: 19 December 2024), with key targets ranked by mean decrease in the Gini index [23]. For SVM, we used the e1071 package (version 1.7.13; usage date: 19 December 2024) and optimized the model to minimize cross-validation error [24]. The number of features contributing to the best model performance was determined, and the top-ranked targets were selected based on their contribution to model accuracy.

Nomogram construction

A nomogram was constructed based on the expression levels of the three core toxicity targets identified (TGFB1, MCL1, and CDKN1A) [25]. Expression data for these targets were extracted from the GSE122897 dataset and analyzed using the rms package (version 6.4.0; usage date: 19 December 2024) in R. Each target was assigned a score based on its relative expression, and the total score was used to predict the risk of IA. The performance of the nomogram was evaluated using Receiver Operating Characteristic (ROC) curve analysis, and the area under the curve (AUC) was calculated to assess predictive accuracy. Additionally, calibration curves and Decision Curve Analysis (DCA) were performed to assess the clinical utility of the nomogram.

Molecular docking analysis

Molecular docking simulations were performed to investigate the interaction between nicotine and the core toxicity targets identified (CDKN1A, MCL1, and TGFB1) [26]. The protein structures were retrieved from the Protein Data Bank (PDB) (https://www.rcsb.org/) (visit date: 20 December 2024), and docking was performed using AutoDock Vina (version 1.1.2; usage date: 20 December 2024) [27]. The protein IDs for these three proteins CDKN1A, MCL1, and TGFB1 are as follows: 5E0U, 2NL9, and 3KFD. The binding affinity of nicotine to each target was assessed by calculating the docking score (Vina score). The interacting residues were identified by visualizing the docking poses in PyMOL (version 2.5.2; usage date: 20 December 2024), and key interactions (hydrogen bonds and hydrophobic interactions) were analyzed [28].

Molecular dynamics simulations

Molecular dynamics simulations were performed employing the Desmond/Maestro 2022.1 software. The simulation environment was prepared using the TIP3P solvation model with a 0.15 M concentration of NaCl to achieve charge neutrality and mimic physiological environments. Initial system optimization involved energy minimization through the steepest descent algorithm to remove steric conflicts and resolve unfavorable atomic overlaps in the starting configuration. Following minimization, the model underwent a 100 ps equilibration phase in the NPT ensemble (300 K, 1 bar) to stabilize thermal and pressure parameters. Subsequently, a production run spanning 100 nanoseconds was conducted under identical thermodynamic parameters. Trajectory data processing and system characterization were accomplished using Desmond's integrated analysis modules, ensuring a comprehensive evaluation of dynamic behaviors.

Immune cell infiltration analysis

Immune cell infiltration levels were estimated using ssGSEA to analyze differences in immune cell populations between IA and normal groups [29]. The analysis was conducted using the GSVA R package (version 1.50.0; usage date: 19 December 2024). Differential infiltration of various immune cell types was evaluated between the two groups. Statistical significance was assessed using the Wilcoxon test ($p < 0.05$). Correlation analyses were performed to assess the relationship between the expression levels of core targets and immune cell populations.

Results

GSVA-based enrichment analysis of DEGs in IA

GSVA was performed on the 5235 DEGs identified between the normal and IA groups from the GSE122897 dataset. The GSVA results revealed significant downregulation of multiple GO terms in the disease group (Figure S1). Significantly downregulated terms comprise "regulation of corticosterone secretion," "response to melanocyte-stimulating hormone," "positive regulation of oxytocin production," "regulation of glycogen metabolic process," "positive regulation of cAMP-mediated signaling," and "glucose homeostasis." Other affected processes include "secretory granule lumen," "cellular pigmentation," "negative regulation of tumor necrosis factor production," "regulation of appetite," "type 4 melanocortin receptor binding," "type 3 melanocortin receptor binding," "neuropeptide signaling pathway," "generation of precursor metabolites and energy," "nervous system development," and "positive regulation of cold-induced thermogenesis." These findings underscore significant alterations in metabolic, secretory, signaling, and homeostatic pathways within IA patients, indicating potential areas for further investigation into the disease's

underlying mechanisms and therapeutic targets. The KEGG enrichment analysis results, depicted in Figure S2, indicate that several pathways are upregulated in the disease group, including those associated with "Prostate cancer," "Chronic myeloid leukemia," "Cell cycle," and "Glioma," which are typically linked to cell proliferation and oncogenic processes. In contrast, numerous pathways were significantly downregulated in the intracranial aneurysm group. These downregulated pathways are predominantly involved in immune response and metabolic regulation, including "Asthma," "Type II diabetes mellitus," "Fc epsilon RI signaling pathway," "T cell receptor signaling pathway," "RIG-I-like receptor signaling pathway," "NOD-like receptor signaling pathway," and "Toll-like receptor signaling pathway." Additional downregulated pathways include "Antigen processing and presentation," "Huntington disease," "Salivary secretion," "Melanogenesis," "Glycerophospholipid metabolism," "Insulin signaling pathway," "Retinol metabolism," "Gap junction," and "Adipocytokine signaling pathway." These findings reveal significant disruptions in immune signaling, metabolic processes, and disease-specific pathways in intracranial aneurysm patients, offering insights into potential molecular mechanisms and therapeutic targets for further research.

WGCNA analysis of DEGs in IA

WGCNA was performed on the expression profiles of the 5235 DEGs identified between normal and IA groups. Figure 2A depicts the module-trait relationships, highlighting the correlation coefficients and their respective p-values for distinct gene modules with each trait. Notably, several modules exhibit strong correlations with IA. Figure 2B illustrates the scatter plot of gene significance for IA versus module membership in the grey module, showing a significant positive correlation ($r = 0.63$, $p = 4.4e\text{-}129$), indicating that genes within this module are highly relevant to IA.

Identification and characterization of common toxic targets between IA and nicotine exposure

From the Grey module, 1127 DEGs were identified. Utilizing data from the CTD, SwissTargetPrediction, and Super-PRED public databases, 637 nicotine-related targets were obtained. As shown in Fig. 3A, a total of 37 overlapping toxic targets related to both IA and nicotine were identified, representing potential key biomarkers or therapeutic targets. The expression patterns of these 37 toxic targets were further investigated. Figure 3B presents a heatmap analysis, highlighting distinct expression profiles between the normal and IA groups. The heatmap illustrates considerable variation in gene expression levels, with several targets showing upregulation or downregulation in IA patients compared to normal controls. Furthermore, a PPI network analysis was conducted for these 37 toxic targets, as depicted in Fig. 3C. The PPI network reveals intricate interactions among key proteins, suggesting potential pathways and mechanisms influenced by nicotine that may contribute to the pathophysiology of IA. Key nodes within the network, such as TNF, CASP3, and HIF1A, indicate central roles in the interaction network, underscoring their significance in IA development in the presence of nicotine. These findings provide insights into the molecular interplay between IA and nicotine exposure, highlighting potential toxicological mechanisms and avenues for therapeutic intervention.

Enrichment analysis of differentially expressed toxicity targets related to nicotine exposure using ssGSEA

To investigate the impact of nicotine exposure on IA at the molecular level, we conducted ssGSEA on 37 identified differentially expressed toxicity targets. As shown in Fig. 4A, the analysis revealed significant differences in several GO biological processes between the normal and IA groups. In comparison to the normal group, the IA group exhibited substantial enrichment in processes related to immune response and inflammation. Specifically, positive regulation of T-helper 1 cell cytokine production, positive regulation of neutrophil extravasation, and response to interleukin-1 were significantly upregulated in the IA group. Additionally, the IA group showed marked elevations in the interleukin-1-mediated signaling pathway, NF-kappaB binding, and regulation of the inflammatory response. Other critical processes showing significant divergence included the Fas signaling pathway, fatty acid oxidation, and activation-induced cell death of T cells. Cell cycle regulation, JNK cascade, and regulation of DNA replication also displayed significant differences, indicating potential disruptions in cell proliferation and stress response mechanisms in IA. KEGG pathway analysis identified several pathways that were significantly altered in the IA group compared to the normal group. Notably, pathways associated with autoimmune and inflammatory diseases, such as Autoimmune thyroid disease, Pathways in cancer, and Non-small cell lung cancer, were significantly upregulated in the IA group (Fig. 4B). Metabolic pathways, including the Adipocytokine signaling pathway, Insulin signaling pathway, and Glycerophospholipid metabolism, were also notably altered. Additionally, key signaling pathways involved in neuronal functions and immune responses, such as the Neurotrophin signaling pathway, TGF-beta signaling pathway, and ubiquitin-mediated proteolysis, exhibited significant differences. The Antigen processing and presentation pathway and Gap junction pathway showed substantial enrichment, further underscoring the involvement of immune and cellular communication processes in the

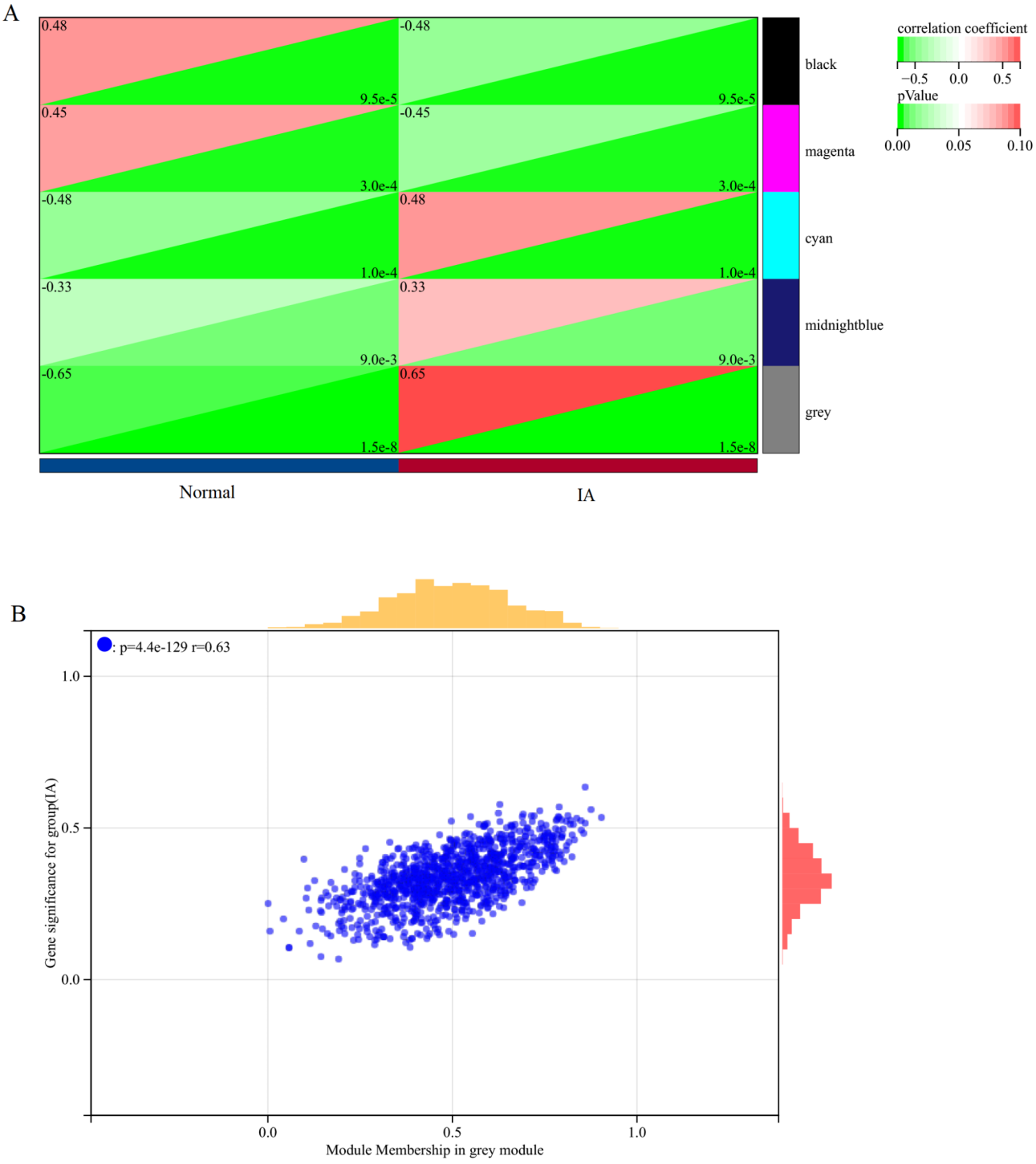

Fig. 2 WGCNA analysis of DEGs in IA. (**A**) Module-trait relationships were determined from WGCNA of DEGs between normal and IA groups. The heatmap displays the correlation coefficients (colored) and their associated p-values for each module's relationship with the traits (normal vs. IA). Positive correlations are indicated in red, and negative correlations are indicated in green. (**B**) Scatter plot of gene significance for IA versus module membership in the grey module

pathology of IA under nicotine exposure. In conclusion, the ssGSEA enrichment analysis highlights a broad spectrum of biological processes and pathways that are differentially regulated in IA in response to nicotine exposure. These findings provide valuable insights into the molecular mechanisms underlying IA and suggest potential therapeutic targets for mitigating the effects of nicotine on IA progression.

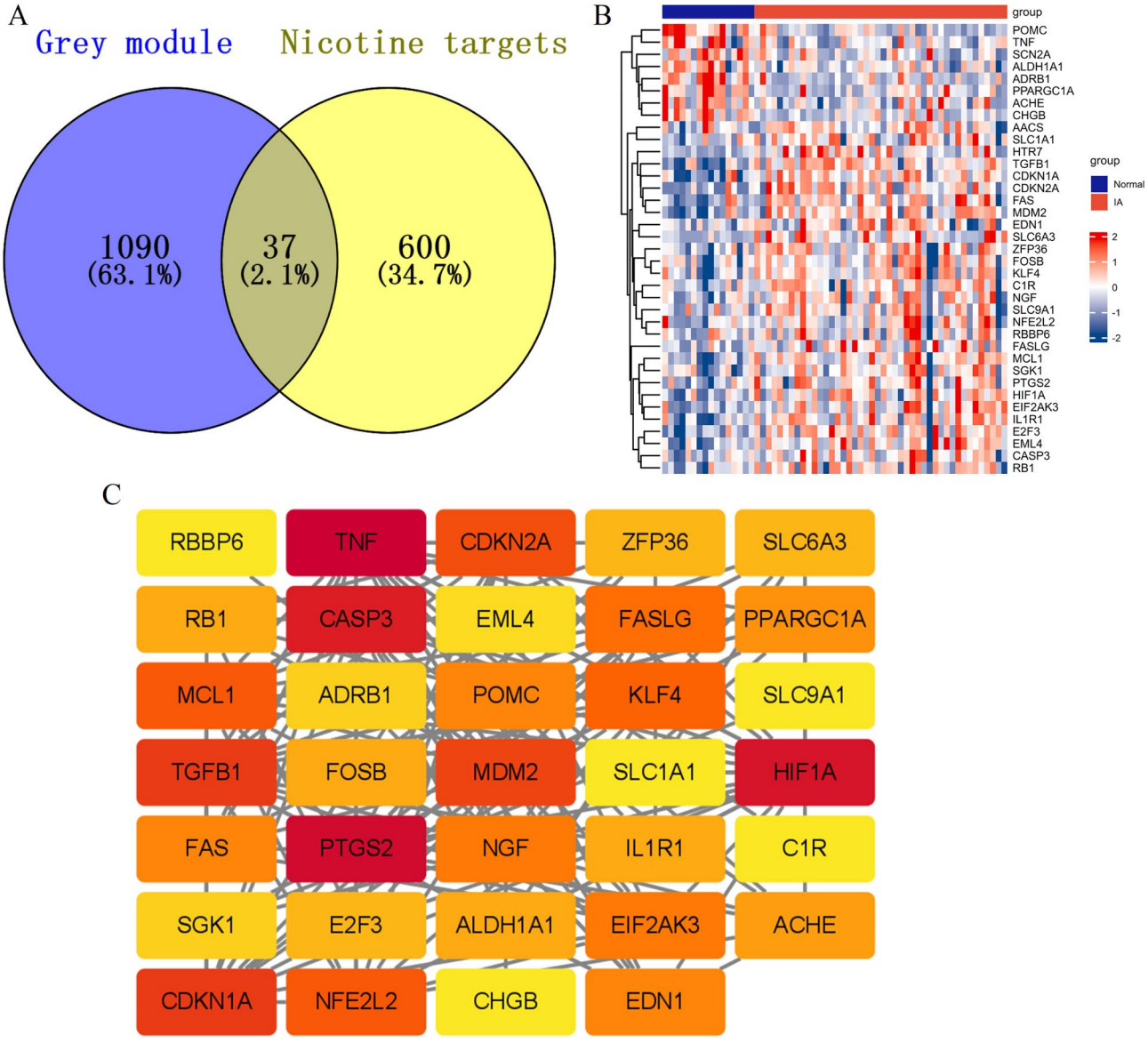

Fig. 3 Identification and analysis of common targets between IA and nicotine-related targets. (**A**) Venn diagram showing the overlap between DEGs in the Grey module and nicotine-related targets. (**B**) Heatmap analysis of the 37 common toxic targets, illustrating the differential expression profiles between normal and IA groups. The color gradient represents the relative expression levels, with red indicating upregulation and blue indicating downregulation. (**C**) PPI network of the 37 common toxic targets. The nodes represent proteins, while the edges represent interactions between them

Identification of key toxicity targets related to nicotine exposure using integrative machine-learning approaches

As shown in Fig. 5A, The application of the RF algorithm identified 8 key toxicity targets, ranked by their mean decrease in the Gini index. Using the SVM algorithm, we identified 24 significant toxicity targets by optimizing the number of features to minimize cross-validation error and maximize accuracy. The number of features corresponding to the minimum error rate (0.17) was 24, while the maximum accuracy rate (0.83) was achieved with 24 features (Fig. 5B and C). The top 10 key nodes in the PPI network were identified based on the degree of connections. Notable targets included TGFB1, MCL1, CDKN1A, and other highly connected proteins such as CASP3, TNF, and HIF1A (Fig. 5D). A Venn diagram integrating the results from RF, SVM, and PPI analyses revealed 3 core toxicity targets (TGFB1, MCL1, and CDKN1A) as critically involved across all methods (Fig. 5E).

Nomogram construction for key toxicity targets in IA

In the GSE122897 dataset, the expression levels of three core toxicity targets were analyzed and compared between normal and IA groups (Fig. 6A). The results showed that the expression levels of CDKN1A, MCL1, and TGFB1 were significantly higher in IA patients

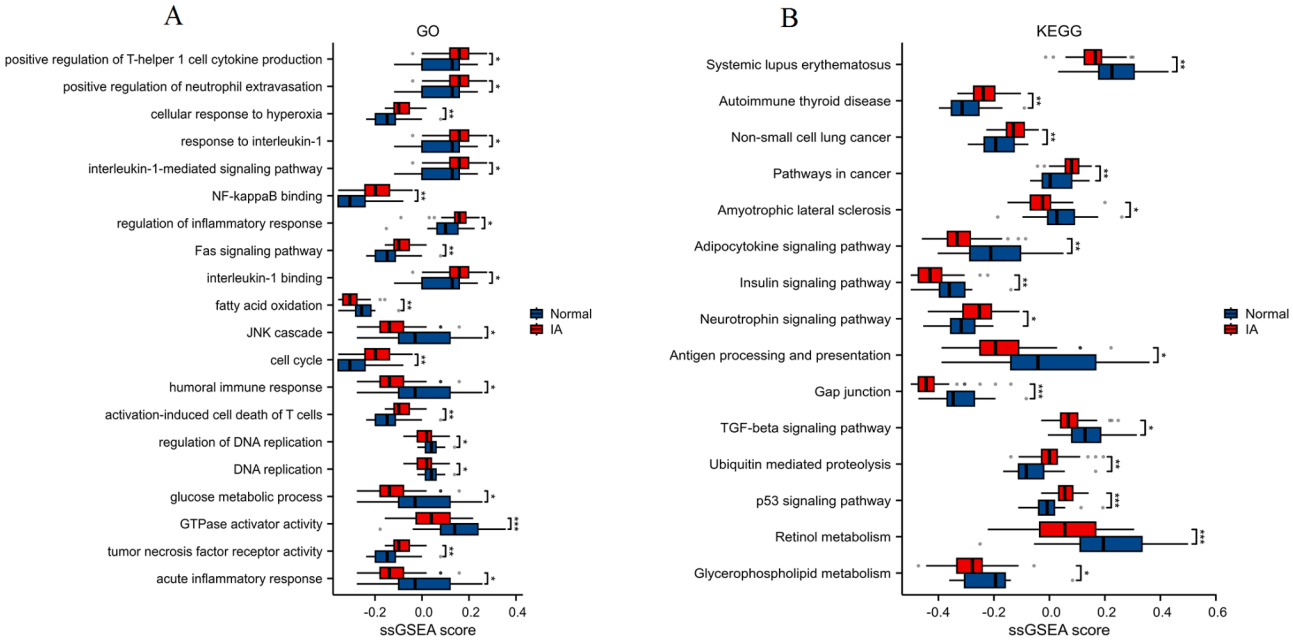

Fig. 4 Enrichment analysis of differentially expressed nicotine-related toxicity targets. (**A**) Box plots represent the ssGSEA scores for various GO terms in the normal and IA groups. (**B**) Box plots show the ssGSEA scores for different KEGG pathways in normal and IA groups. Immune response and inflammation-related processes are upregulated in the IA group. *$p < 0.05$, **$p < 0.01$, ***$p < 0.001$

compared to the normal group ($p < 0.001$ for all genes). A nomogram was constructed based on the expression profiles of the three core targets: TGFB1, MCL1, and CDKN1A (Fig. 6B). Each gene was assigned a score that correlates with its expression level, and the total score was used to predict the risk of IA. The predictive performance of the nomogram was evaluated using ROC analysis, which showed an AUC of 0.852, indicating good predictive accuracy (Fig. 6C). Calibration of the nomogram demonstrated close alignment between predicted and actual probabilities, suggesting reliable predictive performance (Fig. 6D). DCA was also conducted to assess the clinical utility of the nomogram. The DCA curve indicated that the nomogram provides a higher net benefit across a range of risk thresholds compared to the "all" or "none" strategies (Fig. 6E). In summary, the expression analysis confirmed that TGFB1, MCL1, and CDKN1A are significantly upregulated in IA patients. The constructed nomogram based on these core genes exhibited good predictive performance for IA risk, underscoring its potential clinical utility.

Molecular docking analysis of nicotine with core toxicity targets

To assess the interaction between nicotine and the core toxicity targets identified in IA, we performed molecular docking studies. The interaction between nicotine and CDKN1A (Fig. 7A) yielded a Vina score of -5.5, suggesting a moderate binding affinity. Key residues involved in the binding pocket include E55, G34, T51, G127, and H152, which form hydrogen bonds and hydrophobic interactions with nicotine. Docking analysis of nicotine with MCL1 (Fig. 7B) resulted in a Vina score of -5.0, indicating a lower binding affinity than CDKN1A. Important interactions were observed with residues such as E68, F69, Y72, and Y73. These interactions contribute to the stability of the nicotine-MCL1 complex. The docking of nicotine with TGFB1 (Fig. 7C) revealed the strongest binding affinity among the three targets, with a Vina score of -6.0. Crucial residues in the binding site include I42, N44, N14, W52, and I51, which engage in both hydrophobic and polar interactions with nicotine. In summary, molecular docking analysis indicated varying degrees of interaction between nicotine and the core toxicity targets TGFB1, MCL1, and CDKN1A. Among these, TGFB1 exhibited the highest binding affinity, signifying its potential significance in the context of nicotine-induced IA pathology. The results from the molecular dynamics simulation of the nicotine-TGFB1 complex are depicted in Figure S3. The RMSD of the complex (blue line) initially exhibits fluctuations ranging from approximately 2.0 Å to 4.0 Å. After the initial equilibration phase, the protein RMSD stabilizes around 2.5 Å to 4.0 Å with minor fluctuations, indicating a relatively stable conformational state of the nicotine-TGFB1 complex during the simulation period. These molecular dynamics simulation results corroborate the molecular docking predictions, demonstrating that nicotine remains bound to TGFB1.

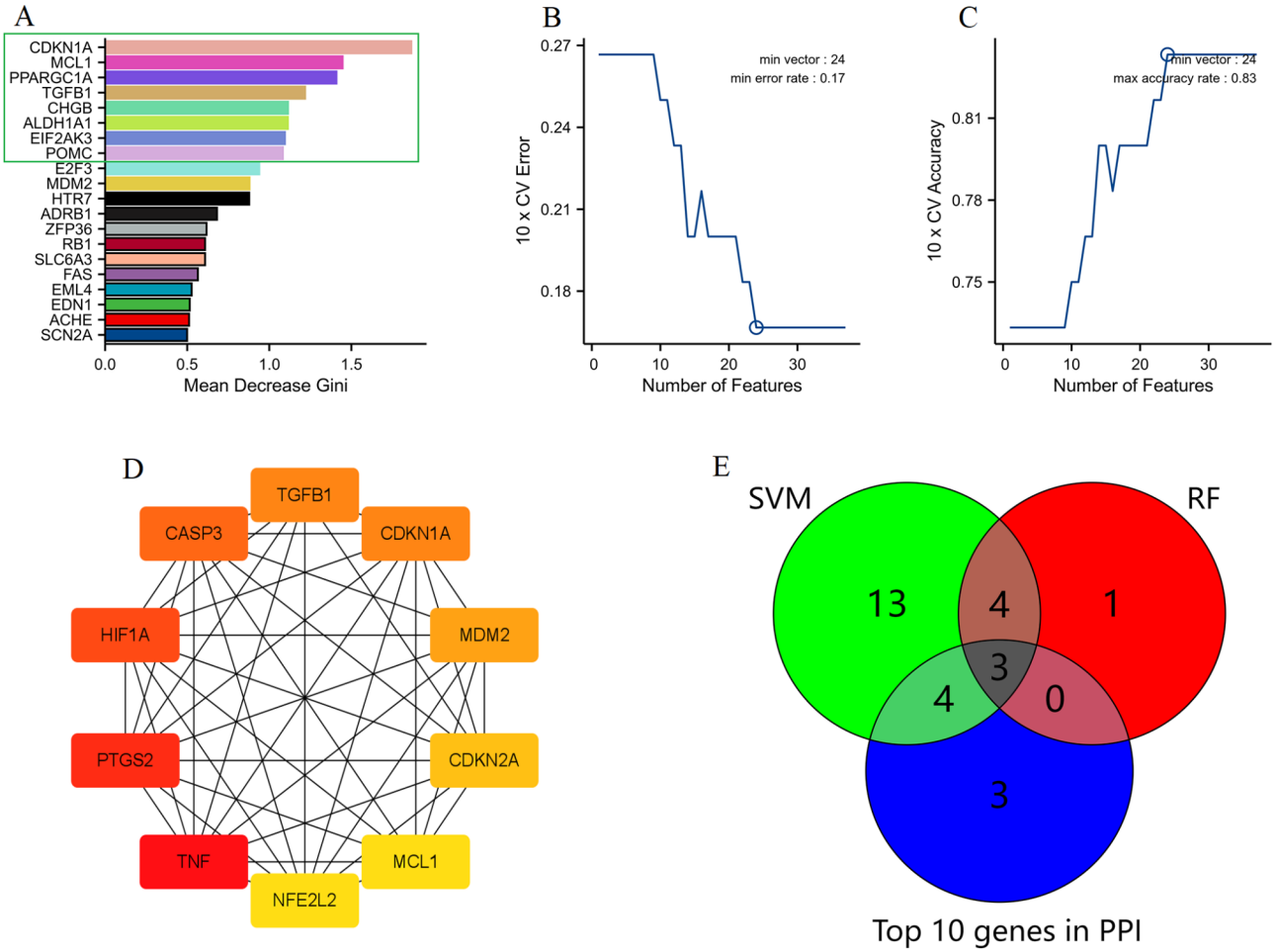

Fig. 5 Identification of key toxicity targets related to nicotine exposure in IA. (**A**) Identification of 8 key toxicity targets using the RF algorithm, ranked by mean decrease in Gini index. (**B**) SVM algorithm performance in terms of cross-validation error across varying numbers of features. (**C**) SVM algorithm performance shows cross-validation accuracy. (**D**) PPI network analysis, identifying the top 10 key nodes based on their degree of connection. (**E**) Venn diagram integrating results from RF, SVM, and PPI analyses

Immune cell infiltration analysis

To investigate the immune landscape associated with IA, we evaluated the immune cell infiltration levels between normal and IA groups using the ssGSEA algorithm. A heatmap representation (Fig. 8A) illustrates the differential infiltration levels of various immune cell types between normal and IA samples. The IA group exhibited a distinct immune infiltration pattern compared to the normal group, with notable differences in several immune cell populations. A quantitative comparison of the ssGSEA scores between normal and IA groups (Fig. 8B) revealed statistically significant differences in specific immune cell populations. Specifically, the IA group showed increased infiltration of immune cells, including aDC, iDC, macrophages, neutrophils, NK CD56dim cells, T cells, Tem, and Th1 cells ($^{*}p<0.05$, $^{**}p<0.01$, $^{***}p<0.001$). Conversely, there was a significant reduction in the infiltration of pDC and TFH in the IA group ($^{*}p<0.05$, $^{**}p<0.01$). Correlation analysis of CDKN1A expression with immune cell infiltration levels (Fig. 9A) revealed significant positive correlations with NK cells ($R=0.422$, $p<0.001$), Th1 cells ($R=0.393$, $p<0.01$), and NK CD56dim cells ($R=0.269$, $p<0.05$). Conversely, CDKN1A expression showed significant negative correlations with TFH cells (R = -0.589, $p<0.001$). The expression of MCL1 exhibited significant positive correlations with several immune cell types, including Th1 cells ($R=0.644$, $p<0.001$), neutrophils ($R=0.491$, $p<0.001$), eosinophils ($R=0.465$, $p<0.001$), and aDC ($R=0.453$, $p<0.001$) (Fig. 9B). Correlation analysis for TGFB1 demonstrated significant positive correlations with NK CD56dim cells ($R=0.612$, $p<0.001$), macrophages ($R=0.388$, $p<0.01$), and aDC ($R=0.378$, $p<0.01$) (Fig. 9C). Significant negative correlations were noted for TFH cells (R = -0.503, $p<0.001$). In summary, the correlation analysis revealed that the expression levels of core toxicity targets CDKN1A, MCL1, and TGFB1 are significantly associated with various immune cell infiltration

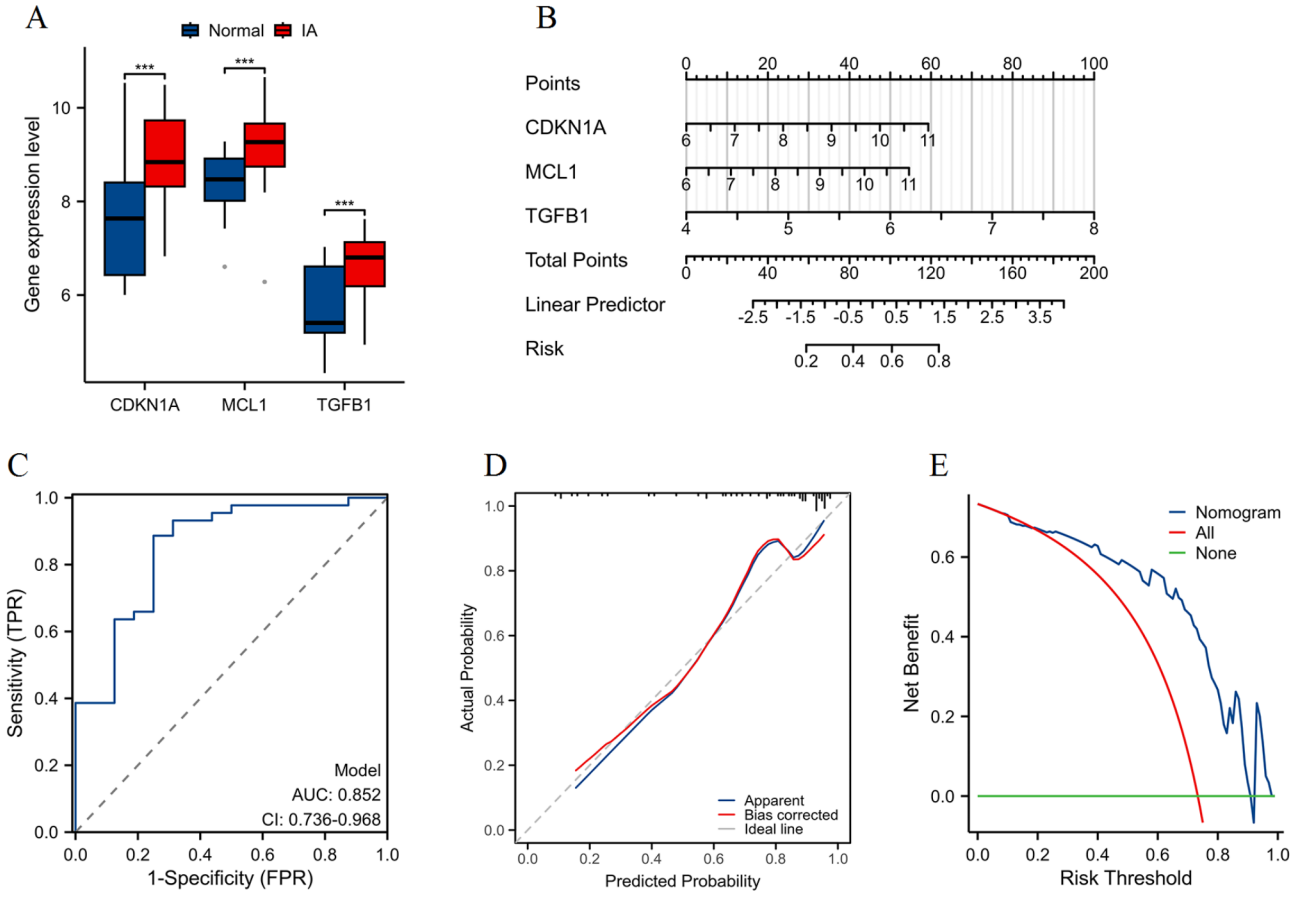

Fig. 6 Nomogram construction for key toxicity targets in IA. (**A**) Gene expression levels of TGFB1, MCL1, and CDKN1A in normal and IA groups from the GSE122897 dataset. Red boxes represent IA samples, blue boxes represent normal samples. *** $p < 0.001$. (**B**) The nomogram was constructed based on the expression profiles of TGFB1, MCL1, and CDKN1A to predict IA risk. (**C**) The receiver operating characteristic (ROC) curve for the nomogram, shows an area under the curve (AUC) of 0.852. (**D**) Calibration plot for the nomogram, demonstrating the agreement between predicted and actual probabilities. (**E**) Decision curve analysis (DCA) shows the net benefit of the nomogram compared to the "all" and "none" strategies across different risk thresholds

levels in IA. These findings suggest that these core genes may play critical roles in modulating the immune microenvironment in IA, influenced by nicotine exposure.

Discussion

IA is a significant vascular condition characterized by the abnormal dilation of arterial walls in the brain, which poses serious health risks due to the potential for rupture. The rupture of an IA can lead to subarachnoid hemorrhage, often resulting in severe neurological deficits or death, making it a critical concern in neurology and vascular health. The prevalence of unruptured IA in the adult population is estimated to be between 2% and 6%, with known risk factors including smoking, hypertension, and genetic predisposition [30]. Understanding the molecular mechanisms underlying IA formation and progression, especially in the context of environmental factors such as nicotine exposure, is essential for developing effective diagnostic and therapeutic strategies [31]. Our findings underscore significant alterations in gene expression and immune responses associated with IA, thereby identifying potential biomarkers and therapeutic targets. Importantly, we have constructed a predictive nomogram based on key toxicity targets related to both IA and nicotine exposure, which could serve as a valuable tool for clinical risk assessment. Furthermore, the integration of advanced bioinformatics methodologies allows for a deeper understanding of the molecular interactions involved in IA pathophysiology, paving the way for future research and improved clinical outcomes.

Our analysis revealed critical changes in immune response and inflammatory pathways in the IA group compared to the normal group. Notably, we observed significant involvement of processes such as the positive regulation of T-helper 1 (Th1) cell cytokine production, neutrophil extravasation, and interleukin-1 (IL-1)-mediated signaling. These results align with previous studies indicating that inflammation plays a crucial role in IA pathophysiology [11, 32]. Several studies have shown that inflammatory cytokines, such as IL-2, TNF-α, IL-1β,

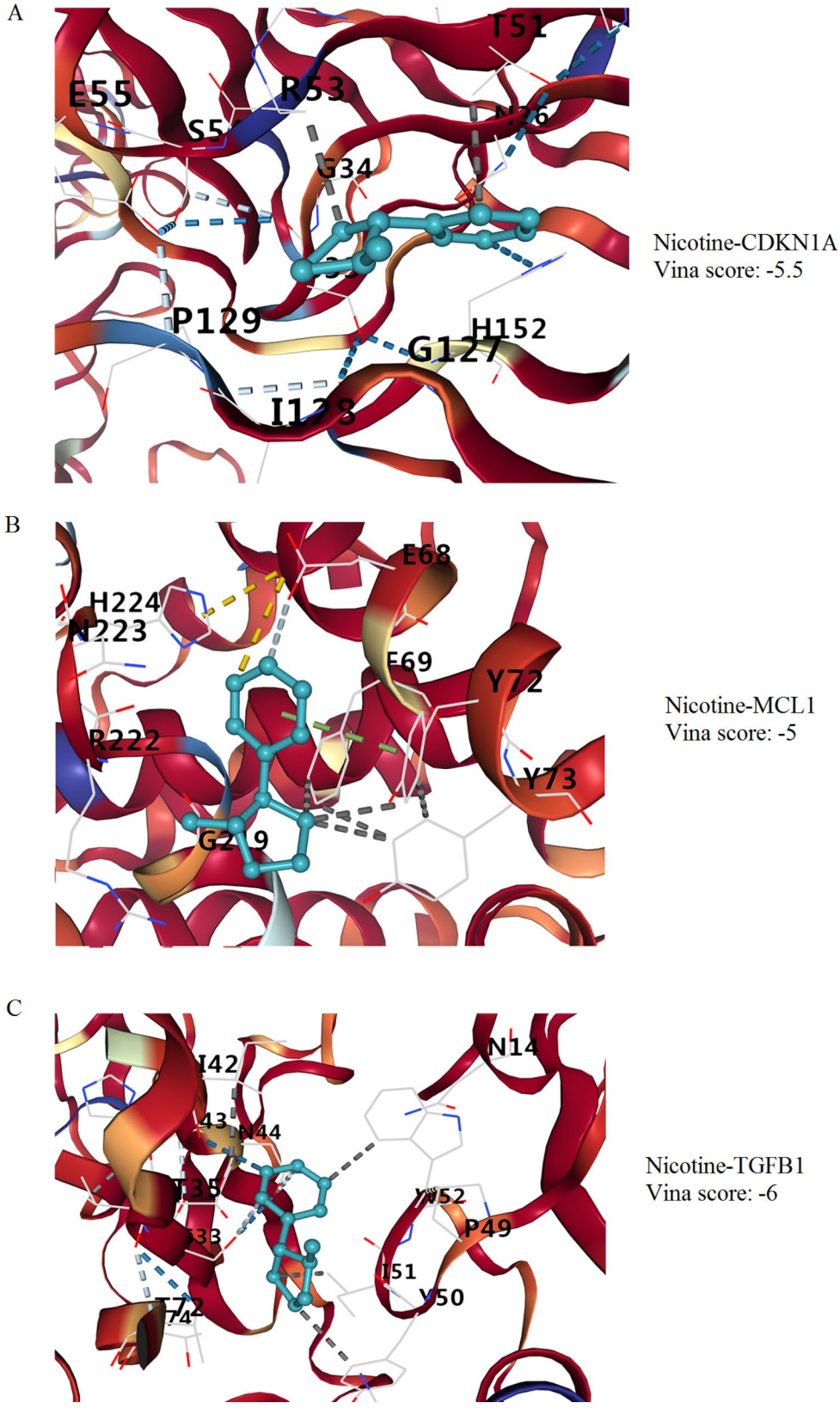

Fig. 7 Molecular docking analysis. (**A**) Interaction of nicotine with CDKN1A. (**B**) Interaction of nicotine with MCL1. (**C**) Interaction of nicotine with TGFB1

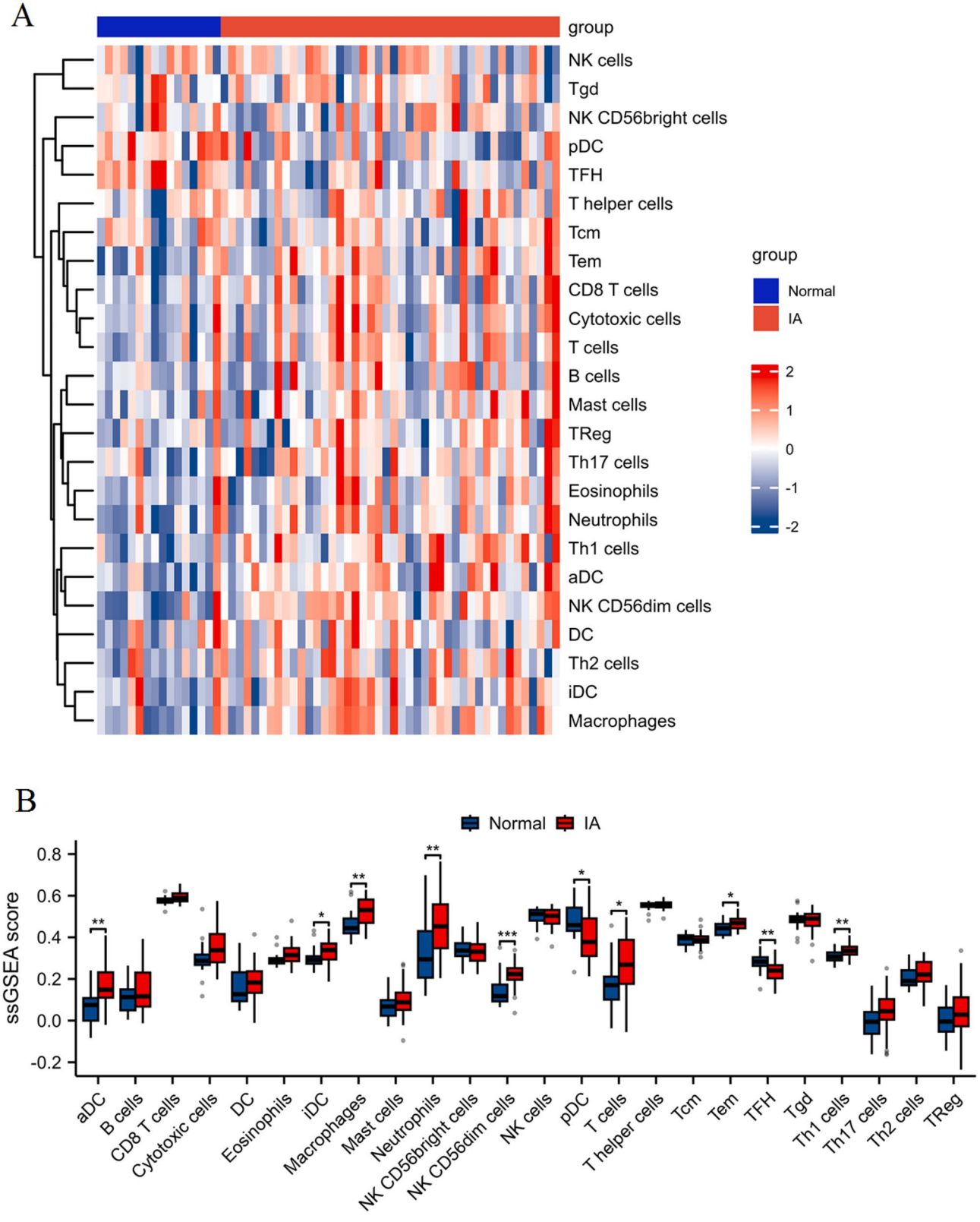

Fig. 8 Immune cell infiltration analysis in IA. (**A**) Heatmap illustrating the differential infiltration levels of various immune cell types between normal (blue) and IA (red) samples. (**B**) Box plots comparing the ssGSEA scores of immune cell populations between normal and IA groups. *$p < 0.05$, **$p < 0.01$, ***$p < 0.001$

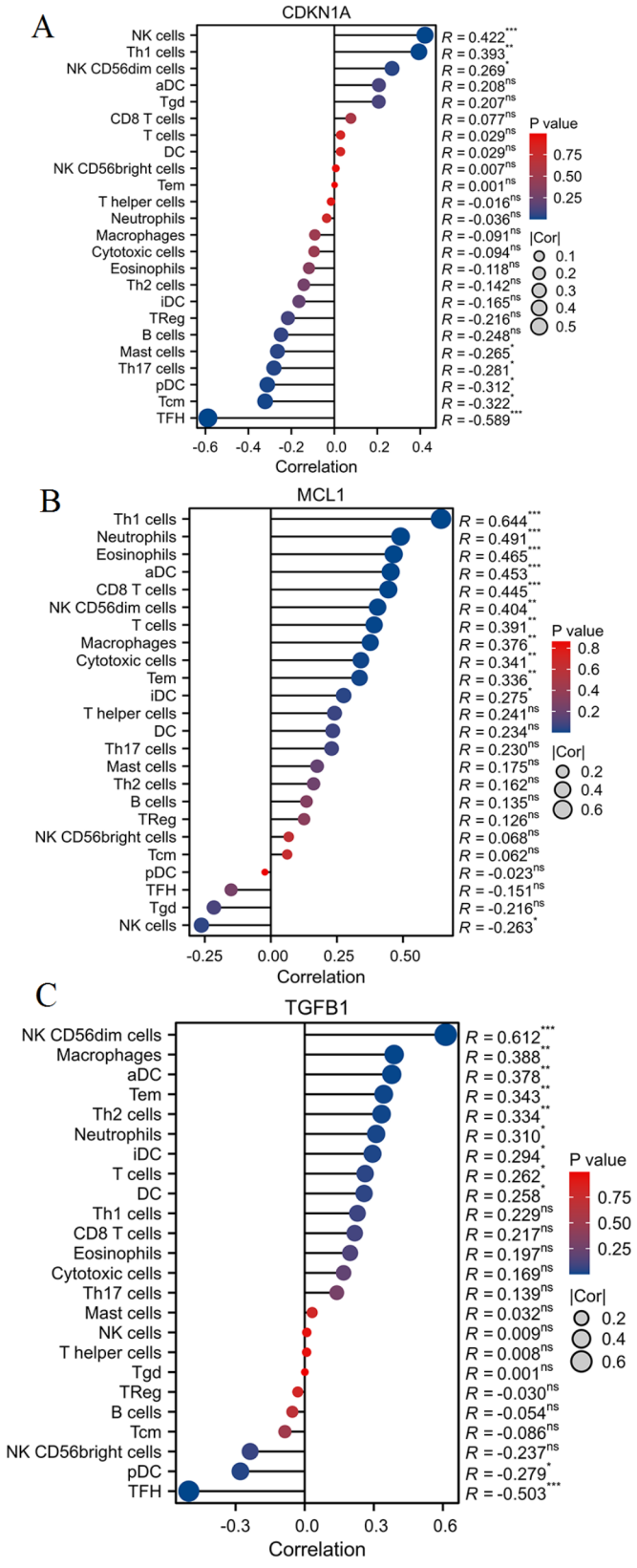

Fig. 9 Correlation between core toxicity targets and Immune cell infiltration levels. (**A**) Correlation analysis between CDKN1A expression and immune cell infiltration levels. (**B**) Correlation analysis between MCL1 expression and immune cell infiltration levels. (**C**) Correlation analysis between TGFB1 expression and immune cell infiltration levels. *$p < 0.05$, **$p < 0.01$, ***$p < 0.001$

MCP-1, and IL-4, are elevated in IA patients and are involved in vascular remodeling and rupture [33, 34]. Specifically, the IL-1 signaling pathway, which exhibited a notable upregulation in our research, has been demonstrated to have the potential for IL-1 to provoke inflammatory responses within the aneurysmal wall. This inflammatory activity may be associated with the rupture of IA [35, 36]. The activation of NF-kappaB signaling, a key regulator of immune and inflammatory responses, is another important finding in our study. Nicotine has been previously implicated in the activation of NF-kappaB in various cell types, including endothelial cells and vascular smooth muscle cells, leading to the production of pro-inflammatory mediators that may exacerbate IA progression [37–39]. Our data corroborate these findings by showing significant enrichment of NF-kappaB binding and inflammatory response regulation in the IA group. This suggests that nicotine may act as a potent modulator of inflammatory pathways in IA, contributing to chronic inflammation and immune cell recruitment, both of which are key factors in aneurysm development and rupture [40, 41].

In addition to immune and inflammatory processes, we identified significant disruptions in metabolic and cellular pathways, including fatty acid oxidation, cell cycle regulation, and DNA replication. These findings highlight the critical role of altered metabolic processes in vascular cells, which have been linked to the pathogenesis of IA. Studies have suggested that endothelial cell metabolism is a key regulator of vascular remodeling and that disruption of metabolic pathways can lead to endothelial dysfunction, a hallmark of aneurysm formation [9, 42]. Our identification of altered fatty acid oxidation and DNA replication pathways in IA under nicotine exposure adds new dimensions to our understanding of the metabolic disruptions that may contribute to the instability of the aneurysmal wall.

Through integrative machine learning approaches, we identified three core toxicity targets (TGFB1, MCL1, and CDKN1A) that were consistently implicated across various analyses and were found to be significantly upregulated in IA patients. These genes demonstrated strong associations with immune cell infiltration, providing further evidence of their involvement in IA pathophysiology. Transforming growth factor-beta 1 (TGFB1) is a key mediator of fibrosis, extracellular matrix remodeling, and immune response regulation. It plays a critical role in vascular smooth muscle cell dysfunction and the formation of aneurysms [43, 44]. Elevated TGFB1 expression in IA patients, as observed in our study, supports its role in modulating the inflammatory environment within the aneurysmal wall. Previous studies have shown that TGFB1 promotes the recruitment of inflammatory cells and the deposition of collagen, leading to the structural remodeling of the vessel wall and potentially facilitating aneurysm growth and rupture [45, 46]. Our findings suggest that TGFB1 could serve as a potential therapeutic target for mitigating the effects of nicotine-induced vascular remodeling in IA. Myeloid cell leukemia-1 (MCL1) is an anti-apoptotic protein that has been shown to protect immune cells from apoptosis and promote cell survival under inflammatory conditions [47, 48]. Our analysis revealed significant positive correlations between MCL1 expression and various immune cell populations, including Th1 cells, neutrophils, and macrophages, suggesting that MCL1 may play a crucial role in sustaining the inflammatory response within the IA microenvironment. This is consistent with studies that have highlighted the role of MCL1 in maintaining chronic inflammation in vascular diseases [49, 50]. Targeting MCL1 could therefore be a promising strategy to modulate immune responses and reduce inflammation in IA patients exposed to nicotine. Cyclin-dependent kinase inhibitor 1 A (CDKN1A), regulates cell cycle progression and plays a key role in cell cycle arrest and DNA damage response [51]. Our correlation analysis revealed significant associations between CDKN1A expression and various immune cell populations, including NK cells and Th1 cells. This suggests that CDKN1A may not only influence cell cycle regulation in vascular cells but also modulate immune cell activation and proliferation within the aneurysmal microenvironment. CDKN1A is involved in immune response regulation in several inflammatory diseases, and its upregulation in IA could contribute to chronic inflammation and immune cell dysregulation [52, 53]. Targeting CDKN1A could potentially restore immune homeostasis and mitigate the inflammatory response in IA patients.

The activation of macrophages and the inflammatory response are vital factors in the development and advancement of IA [54]. Our immune cell infiltration analysis revealed significant changes in the immune landscape of IA, with increased infiltration of pro-inflammatory immune cells, including macrophages, neutrophils, and Th1 cells, and a concomitant reduction in the infiltration of regulatory cells such as TFH cells and pDC. This altered immune cell profile suggests that nicotine exposure may shift the immune response in IA towards a more pro-inflammatory and Th1-dominant phenotype, which has been associated with the progression of various vascular diseases, including IA [33, 34, 55]. The increased presence of macrophages and neutrophils, which are known to release pro-inflammatory cytokines and reactive oxygen species, further supports the idea that nicotine-induced inflammation plays a key role in the pathogenesis of IA [56, 57].

Finally, the construction of a predictive nomogram based on the expression levels of TGFB1, MCL1, and

CDKN1A, achieving an AUC of 0.852 in ROC analysis, represents a significant step forward in clinical decision-making for IA risk assessment. This nomogram could enhance the ability to predict IA and guide future research toward validating and refining this model for broader clinical application. The integration of such predictive tools into routine clinical practice holds promise for improving patient outcomes and individualized care strategies.

The limitations of this study should be acknowledged, as they may impact the interpretation of the results. Firstly, the relatively small sample size may limit the generalizability of the identified differentially expressed genes and pathways. Additionally, without clinical validation analyses, the clinical applicability of our findings remains uncertain. These limitations highlight the need for further research to corroborate our findings and explore the clinical implications.

Conclusions

In conclusion, this study demonstrates significant alterations in gene expression and immune responses associated with intracranial aneurysm under nicotine exposure, while successfully identifying key toxicity targets and developing a predictive nomogram. These findings not only enhance our understanding of the molecular mechanisms underlying IA but also pave the way for targeted interventions and improved risk assessment strategies in its management. Future research should focus on validating these results through experimental approaches and exploring their clinical applications, thereby contributing to more effective therapeutic strategies for patients affected by IA.

Supplementary Information

The online version contains supplementary material available at https://doi.org/10.1186/s40360-025-00921-3.

Supplementary Material 1

Supplementary Material 2

Acknowledgements
Not applicable.

Author contributions
Qiang Ma wrote the manuscript and designed the study. Data analysis and figure creation were handled by Longnian Zhou. The manuscript was reviewed and edited by Zhongde Li. All authors contributed to the study and approved the final version of the manuscript.

Funding
Not applicable.

Data availability
Data is provided within the manuscript or supplementary information files.

Declarations

Ethics approval and consent to participate
Not applicable.

Consent for publication
Not applicable.

Competing interests
The authors declare no competing interests.

Received: 2 January 2025 / Accepted: 8 April 2025
Published online: 17 April 2025

References

1. Etminan N, Dörfler A, Steinmetz H. Unruptured intracranial Aneurysms-pathogenesis and individualized management. Deutsches Arzteblatt Int. 2020;117(14):235–42.
2. Rahmani R, Baranoski JF, Albuquerque FC, Lawton MT, Hashimoto T. Intracranial aneurysm calcification - A narrative review. Exp Neurol. 2022;353:114052.
3. Malhotra A, Wu X, Forman HP, Matouk CC, Hughes DR, Gandhi D, Sanelli P. Management of unruptured intracranial aneurysms in older adults: A Cost-effectiveness analysis. Radiology. 2019;291(2):411–7.
4. Lee KS, Zhang JJY, Nguyen V, Han J, Johnson JN, Kirollos R, Teo M. The evolution of intracranial aneurysm treatment techniques and future directions. Neurosurg Rev. 2022;45(1):1–25.
5. Pontes FGB, da Silva EM, Baptista-Silva JC, Vasconcelos V. Treatments for unruptured intracranial aneurysms. Cochrane Database Syst Rev. 2021;5(5):Cd013312.
6. Karhunen V, Bakker MK, Ruigrok YM, Gill D, Larsson SC. Modifiable risk factors for intracranial aneurysm and aneurysmal subarachnoid hemorrhage: A Mendelian randomization study. J Am Heart Association. 2021;10(22):e022277.
7. Ya X, Zhang C, Zhang S, Zhang Q, Cao Y, Wang S, Zhao J. The relationship between smoking and delayed cerebral ischemia after intracranial aneurysm rupture: A systematic review and Meta-Analysis. Front Neurol. 2021;12:625087.
8. Tanji F, Nanbu H, Fushimi S, Shibata K, Kondo R. Smoking status and unruptured intracranial aneurysm among brain health check-up examinees: a cross-sectional study in Japan. J Rural Medicine: JRM. 2020;15(4):183–8.
9. Sheinberg DL, McCarthy DJ, Elwardany O, Bryant JP, Luther E, Chen SH, Thompson JW, Starke RM. Endothelial dysfunction in cerebral aneurysms. NeuroSurg Focus. 2019;47(1):E3.
10. Luo L, Ma X, Kong D, Dai Y, Li T, Yu H, Liu J, Li M, Xu Y, Xiang G, et al. Multiomics integrated analysis and experimental validation identify TLR4 and ALOX5 as oxidative stress-related biomarkers in intracranial aneurysms. J Neuroinflamm. 2024;21(1):225.
11. Jin J, Duan J, Du L, Xing W, Peng X, Zhao Q. Inflammation and immune cell abnormalities in intracranial aneurysm subarachnoid hemorrhage (SAH): relevant signaling pathways and therapeutic strategies. Front Immunol. 2022;13:1027756.
12. Kamio Y, Miyamoto T, Kimura T, Mitsui K, Furukawa H, Zhang D, Yokosuka K, Korai M, Kudo D, Lukas RJ, et al. Roles of nicotine in the development of intracranial aneurysm rupture. Stroke. 2018;49(10):2445–52.
13. Ogilvy CS, Gomez-Paz S, Kicielinski KP, Salem MM, Akamatsu Y, Waqas M, Rai HH, Catapano JS, Muram S, Elghareeb M, et al. Cigarette smoking and risk of intracranial aneurysms in middle-aged women. J Neurol Neurosurg Psychiatry. 2020;91(9):985–90.
14. Chen C, Yang K, Zhang Y, Lu M, Zhao X, Wan Z. Pathogenic gene connections in type 2 diabetes and non-alcoholic fatty liver disease: a bioinformatics analysis and mouse model investigations experiments. Nutr Diabetes. 2024;14(1):60.
15. Su C, Lin Z, Ye Z, Liang J, Yu R, Wan Z, Hou J. Development of a prognostic model for early-stage gastric cancer-related DNA methylation-driven genes and analysis of immune landscape. Front Mol Biosci. 2024;11:1455890.
16. Ding R, Liang D, Huang S, Huang X, Wei B, Wan S, Zhang H, Wan Z. Utilising bioinformatics and systems biology methods to uncover the impact of dermatomyositis on interstitial lung disease. Clinical and experimental rheumatology 2025.

17. Ritchie ME, Phipson B, Wu D, Hu Y, Law CW, Shi W, Smyth GK. Limma powers differential expression analyses for RNA-sequencing and microarray studies. Nucleic Acids Res. 2015;43(7):e47.
18. Hänzelmann S, Castelo R, Guinney J. GSVA: gene set variation analysis for microarray and RNA-seq data. BMC Bioinformatics. 2013;14:7.
19. Langfelder P, Horvath S. WGCNA: an R package for weighted correlation network analysis. BMC Bioinformatics. 2008;9:559.
20. Davis AP, Wiegers TC, Johnson RJ, Sciaky D, Wiegers J, Mattingly CJ. Comparative toxicogenomics database (CTD): update 2023. Nucleic Acids Res. 2023;51(D1):D1257–62.
21. Daina A, Michielin O, Zoete V. SwissTargetPrediction: updated data and new features for efficient prediction of protein targets of small molecules. Nucleic Acids Res. 2019;47(W1):W357–64.
22. Shannon P, Markiel A, Ozier O, Baliga NS, Wang JT, Ramage D, Amin N, Schwikowski B, Ideker T. Cytoscape: a software environment for integrated models of biomolecular interaction networks. Genome Res. 2003;13(11):2498–504.
23. Safia Naveed S. Prediction of breast cancer through random forest. Curr Med Imaging. 2023;19(10):1144–55.
24. Huang S, Cai N, Pacheco PP, Narrandes S, Wang Y, Xu W. Applications of support vector machine (SVM) learning in cancer genomics. Cancer Genomics Proteomics. 2018;15(1):41–51.
25. Wu J, Zhang H, Li L, Hu M, Chen L, Xu B, Song Q. A nomogram for predicting overall survival in patients with low-grade endometrial stromal sarcoma: A population-based analysis. Cancer Commun (London England). 2020;40(7):301–12.
26. Pinzi L, Rastelli G. Molecular docking: shifting paradigms in drug discovery. Int J Mol Sci. 2019;20(18).
27. Burley SK, Berman HM, Kleywegt GJ, Markley JL, Nakamura H, Velankar S. Protein data bank (PDB): the single global macromolecular structure archive. Methods in molecular biology. (Clifton NJ). 2017;1607:627–41.
28. Seeliger D, de Groot BL. Ligand Docking and binding site analysis with PyMOL and Autodock/Vina. J Comput Aided Mol Des. 2010;24(5):417–22.
29. Bindea G, Mlecnik B, Tosolini M, Kirilovsky A, Waldner M, Obenauf AC, Angell H, Fredriksen T, Lafontaine L, Berger A, et al. Spatiotemporal dynamics of intratumoral immune cells reveal the immune landscape in human cancer. Immunity. 2013;39(4):782–95.
30. Tromp G, Weinsheimer S, Ronkainen A, Kuivaniemi H. Molecular basis and genetic predisposition to intracranial aneurysm. Ann Med. 2014;46(8):597–606.
31. Guo X, Wu Y, Fang J. Misdiagnosis of a dissecting aneurysm as a cerebral aneurysm: A preoperative case report. Altern Ther Health Med. 2023;29(8):663–7.
32. Gruszka W, Zbroszczyk M, Komenda J, Gruszczyńska K, Baron J. The role of inflammation and potential Pharmacological therapy in intracranial aneurysms. Neurol Neurochir Pol. 2018;52(6):662–9.
33. Kamińska J, Maciejczyk M, Ćwiklińska A, Matowicka-Karna J, Koper-Lenkiewicz OM. Pro-Inflammatory and Anti-Inflammatory cytokines levels are significantly altered in cerebrospinal fluid of unruptured intracranial aneurysm (UIA) patients. J Inflamm Res. 2022;15:6245–61.
34. Zhang HF, Zhao MG, Liang GB, Song ZQ, Li ZQ. Expression of pro-inflammatory cytokines and the risk of intracranial aneurysm. Inflammation. 2013;36(6):1195–200.
35. Liu Q, Liu P, Zhang Y, Mossa-Basha M, Hasan DM, Li J, Zhu C, Wang S. Serum Interleukin-1 levels are associated with intracranial aneurysm instability. Translational Stroke Res. 2024;15(2):433–45.
36. Wen Z, Liu Q, Jiang P, Zhu C, Li J, Wu J, Wang S, Ning B. Serum interleukin-1 is a new biomarker to predict the risk of rebleeding of ruptured intracranial aneurysm after admission. Neurosurg Rev. 2023;46(1):123.
37. Lian S, Li S, Zhu J, Xia Y, Do Jung Y. Nicotine stimulates IL-8 expression via ROS/NF-κB and ROS/MAPK/AP-1 axis in human gastric cancer cells. Toxicology. 2022;466:153062.
38. AlQasrawi D, Naser E, Naser SA. Nicotine increases macrophage survival through α7nAChR/NF-κB pathway in mycobacterium avium paratuberculosis infection. Microorganisms. 2021;9(5).
39. Wang C, Gu W, Zhang Y, Ji Y, Wen Y, Xu X. Nicotine promotes cervical carcinoma cell line HeLa migration and invasion by activating PI3k/Akt/NF-κB pathway in vitro. Experimental Toxicologic Pathology: Official J Gesellschaft fur Toxikologische Pathologie. 2017;69(6):402–7.
40. Zhang W, Xiang C, Liu B, Hou F, Zheng Z, Chen Z, Suo L, Feng G, Gu J. The value of systemic immune inflammation index, white blood cell to platelet ratio, and homocysteine in predicting the instability of small saccular intracranial aneurysms. Sci Rep. 2024;14(1):24312.
41. Zeyu Z, Yuanjian F, Cameron L, Sheng C. The role of immune inflammation in aneurysmal subarachnoid hemorrhage. Exp Neurol. 2021;336:113535.
42. Ono I, Abekura Y, Kawashima A, Oka M, Okada A, Hara S, Miyamoto S, Kataoka H, Ishii A, Yamamoto K, et al. Endothelial cell malfunction in unruptured intracranial aneurysm lesions revealed using a 3D-casted mold. J Neuropathol Exp Neurol. 2022;82(1):49–56.
43. Zhu C, Ying D, Zhou D, Mi J, Zhang W, Chang Q, Li L. Expression of TGF-beta1 in smooth muscle cells regulates endothelial progenitor cells migration and differentiation. J Surg Res. 2005;125(2):151–6.
44. Pei H, Tian C, Sun X, Qian X, Liu P, Liu W, Chang Q. Overexpression of MicroRNA-145 promotes ascending aortic aneurysm media remodeling through TGF-β1. Eur J Vascular Endovascular Surgery: Official J Eur Soc Vascular Surg. 2015;49(1):52–9.
45. Jones JA, Spinale FG, Ikonomidis JS. Transforming growth factor-beta signaling in thoracic aortic aneurysm development: a paradox in pathogenesis. J Vasc Res. 2009;46(2):119–37.
46. Kothapalli CR, Ramamurthi A. Induced Elastin regeneration by chronically activated smooth muscle cells for targeted aneurysm repair. Acta Biomater. 2010;6(1):170–8.
47. Cui J, Placzek WJ. PTBP1 enhances miR-101-guided AGO2 targeting to MCL1 and promotes miR-101-induced apoptosis. Cell Death Dis. 2018;9(5):552.
48. Wang S, Cheng Z, Chen X, Lu G, Zhu X, Xu G. CircUBXN7 mitigates H/R-induced cell apoptosis and inflammatory response through the miR-622-MCL1 axis. Am J Translational Res. 2021;13(8):8711–27.
49. Huang J, Hong L, Shen B, Zhou Y, Lan J, Peng Y. FOXO1 represses MCL1 transcription to regulate the function of vascular smooth muscle cells in intracranial aneurysm. Exp Brain Res. 2022;240(11):2861–70.
50. Torres-Adorno AM, Lee J, Kogawa T, Ordentlich P, Tripathy D, Lim B, Ueno NT. Histone deacetylase inhibitor enhances the efficacy of MEK inhibitor through NOXA-Mediated MCL1 degradation in Triple-Negative and inflammatory breast cancer. Clin cancer Research: Official J Am Association Cancer Res. 2017;23(16):4780–92.
51. Kleinsimon S, Longmuss E, Rolff J, Jäger S, Eggert A, Delebinski C, Seifert G. GADD45A and CDKN1A are involved in apoptosis and cell cycle modulatory effects of viscumtt with further inactivation of the STAT3 pathway. Sci Rep. 2018;8(1):5750.
52. Allouch A, Voisin L, Zhang Y, Raza SQ, Lecluse Y, Calvo J, Selimoglu-Buet D, de Botton S, Louache F, Pflumio F, et al. CDKN1A is a target for phagocytosis-mediated cellular immunotherapy in acute leukemia. Nat Commun. 2022;13(1):6739.
53. Hu K, Li J, Wu G, Zhou L, Wang X, Yan Y, Xu Z. The novel roles of virus infection-associated gene CDKN1A in chemoresistance and immune infiltration of glioblastoma. Aging. 2021;13(5):6662–80.
54. Duan J, Zhao Q, He Z, Tang S, Duan J, Xing W. Current Understanding of macrophages in intracranial aneurysm: relevant etiological manifestations, signaling modulation and therapeutic strategies. Front Immunol. 2023;14:1320098.
55. Zhang HF, Zhao MG, Liang GB, Yu CY, He W, Li ZQ, Gao X. Dysregulation of CD4(+) T cell subsets in intracranial aneurysm. DNA Cell Biol. 2016;35(2):96–103.
56. Roxlau ET, Pak O, Hadzic S, Garcia-Castro CF, Gredic M, Wu CY, Schäffer J, Selvakumar B, Pichl A, Spiegelberg D, et al. Nicotine promotes e-cigarette vapour-induced lung inflammation and structural alterations. Eur Respir J. 2023;61(6).
57. Belkin S, Benthien J, Axt PN, Mohr T, Mortensen K, Weckmann M, Drömann D, Franzen KF. Impact of heated tobacco products, E-Cigarettes, and cigarettes on inflammation and endothelial dysfunction. Int J Mol Sci. 2023;24(11).

Publisher's note